JOTCS A
Journal of the Turkish Chemical Society
Section: A
Chemistry

TURKISH CHEMICAL SOCIETY

Effect of Terminal Donor Units on the Electronic and Photovoltaic Properties of Conjugated Small Molecules: A DFT/TD-DFT Study

Pınar Seyitdanlıoğlu[1], Hilal Kalkan[2*]

[1]Hacettepe University, Faculty of Science, Department of Chemistry, Ankara, 06800, Türkiye.
[2]Gazi University, Scientific Research Projects Unit, Ankara, 06500, Türkiye.

Abstract: Isoindigo-based donor–acceptor small molecules are promising candidates for organic photovoltaic applications because of their strong electron-accepting character and tunable π-conjugated structures. In this work, seven isoindigo-based derivatives bearing phenyl, thiophene, thiophene, benzothiophene, fluorene, carbazole, phenoxazine, and julolidine terminal donor units were computationally designed and investigated using density functional theory (DFT) and time-dependent DFT (TD-DFT) calculations. Following a benchmark study, B3PW91/6-31+G(d,p) was selected for the systematic evaluation of structural, electronic, optical, and OPV-related properties. The results indicate that donor modification mainly affects the highest occupied molecular orbital (HOMO) energy, while the lowest unoccupied molecular orbital (LUMO) remains largely localized on the isoindigo acceptor core. Stronger donor units narrowed the electronic gap and induced bathochromic shifts in absorption, but excessive HOMO destabilization decreased the estimated open-circuit voltage from 1.28 to 0.59 V. Among the investigated molecules, the benzothiophene derivative **I3** showed the most balanced OPV-related descriptor profile, with λ_{max} = 672.55 nm, f = 1.67, LHE = 0.98, E_b = 0.36 eV, ΔLUMO = 0.64 eV, and an estimated V_{oc} of 1.27 V. In contrast, phenoxazine and julolidine derivatives exhibited more strongly red-shifted absorption maxima at 803 and 838 nm, respectively, but their less favorable voltage-related descriptors and higher exciton binding energies reduced their overall OPV-related descriptor balance. These findings indicate that moderate donor strength is more favorable than excessive electron donation for achieving a balance among absorption, exciton dissociation, and voltage retention in isoindigo-based small-molecule OPV candidates.

Keywords: Isoindigo derivatives, Donor–acceptor systems, Organic photovoltaics, DFT/TD-DFT, Structure–property relationships.

Submitted: May 6, 2026. **Accepted:** August 21, 2026.

Cite this: Seyitdanlıoğlu P, Kalkan H. Effect of Terminal Donor Units on the Electronic and Photovoltaic Properties of Conjugated Small Molecules: A DFT/TD-DFT Study. JOTCSA. 2026; 2026(2):**1945490**, 1-16.

DOI: https://doi.org/10.18596/jotcsa.1945490

Izlik page: https://izlik.org/JA48YY95EN

***Corresponding author's E-mails:** hilalkalkan@gazi.edu.tr

1. INTRODUCTION

The development of structurally tunable organic semiconductors remains an important strategy for improving organic photovoltaic (OPV) materials. Compared with their inorganic counterparts, organic materials offer advantages such as solution processability, low-cost fabrication, structural flexibility, and compatibility with lightweight and flexible devices (1–4). Among the various molecular design strategies, donor–acceptor (D–A) architectures are particularly attractive because the electronic interaction between electron-rich and electron-deficient units enables systematic tuning of frontier molecular orbital energies, optical gaps, absorption profiles, and charge-transfer character (5–8).

In this context, isoindigo has attracted considerable attention as an electron-deficient building block for π-conjugated OPV materials. Its lactam-containing rigid conjugated structure provides strong electron-accepting character, favorable planarity, and low-lying LUMO energy levels, which are beneficial for visible-to-near-infrared absorption and donor–acceptor electronic communication (9–15). However, OPV performance is not governed solely by the electronic structure of isolated molecules.

Intermolecular packing, π–π stacking, side-chain engineering, blend morphology, and charge transport also play decisive roles in real devices (16–19). Therefore, molecular-level calculations should be interpreted as screening tools that provide structure–property relationships rather than direct device-performance predictions.

Although isoindigo-based materials have been widely investigated in polymeric systems, structurally defined small-molecule analogues have been less systematically explored. Symmetric donor–acceptor–donor (D–A–D) small molecules are useful model systems because terminal donor units can be varied within the same molecular framework, allowing the effects of terminal donors on electronic structure and optical response to be directly compared (20–23). Such comparisons are valuable for identifying how donor strength influences the balance among absorption red-shift, exciton dissociation, and voltage retention.

In this work, we designed seven isoindigo-based D–A–D small molecules bearing phenyl, thiophene, benzothiophene, fluorene, carbazole, phenoxazine, and julolidine terminal donor units. Using a consistent DFT/TD-DFT protocol, we investigated optimized geometries, frontier molecular orbitals, orbital localization, low-energy electronic transitions, and OPV-related descriptors including HOMO–LUMO gap, absorption maximum, oscillator strength, light-harvesting efficiency, estimated V_{oc}, LUMO offset, and exciton binding energy. The main objective was to establish donor-dependent structure–property relationships and to identify donor units that provide a balanced compromise between red-shifted absorption and voltage preservation in isoindigo-based small-molecule OPV candidates.

2. COMPUTATIONAL DETAILS

All quantum chemical calculations were performed using DFT and TD-DFT as implemented in Gaussian 16 (24), and all molecular visualizations were generated using GaussView 6 (25). The molecular structures were constructed and subsequently fully optimized without imposing any symmetry constraints. Before the systematic evaluation of the molecular series, a benchmark study was carried out on the reference compound to identify a suitable computational protocol. The molecules were then fully optimized at the B3PW91/6-31+G(d,p) level (26-29). Vibrational frequency calculations were performed at the same level of theory to confirm that the optimized structures corresponded to true minima on the potential energy surface. The absence of imaginary frequencies confirmed that all optimized geometries corresponded to local minima. These optimized geometries were subsequently used for frontier molecular orbital analysis, TD-DFT calculations, structural evaluation, and photovoltaic descriptor estimation.

The HOMO and LUMO energies were obtained from the optimized ground-state geometries. TD-DFT calculations were performed on the optimized ground-state geometries to obtain vertical excitation energies, absorption wavelengths, and oscillator strengths. The optical excitation energy (E_{opt}) was taken directly from the first singlet excitation energy reported in the TD-DFT output. Therefore, E_{opt} represents the lowest vertical electronic excitation energy of each molecule. The absorption wavelengths and oscillator strengths obtained from TD-DFT calculations were used to characterize the optical response of the investigated systems.
The LHE was estimated from the oscillator strength according to:

$$LHE = 1 - 10^{-f}$$

where f is the oscillator strength of the selected electronic transition. To ensure consistent comparison across the molecular series, the same transition-selection criterion was applied to all derivatives. In the main descriptor table, LHE values were calculated using the oscillator strength associated with the main low-energy absorption maximum obtained from TD-DFT calculations. Where relevant, visible-region oscillator strengths were discussed separately as additional indicators of visible-light absorption, but they were not used to replace the main LHE descriptor (30).

The V_{oc} was estimated using the donor–acceptor energy-level relationship:

$$V_{oc} = |E_{HOMO}^{donor}| - |E_{LUMO}^{acceptor}| - 0.30$$

where E_{HOMO}^{donor} is the HOMO energy of the investigated donor molecule and $E_{LUMO}^{acceptor}$ is the LUMO energy of the reference acceptor (31). A reference acceptor LUMO level of −3.95 eV was used in this study (32). The empirical energy-loss term of 0.30 eV was included to account for interfacial and energetic losses commonly considered in theoretical OPV screening. It should be noted that this Scharber-type expression provides a simplified molecular-level estimate and should not be interpreted as a direct prediction of the device-level open-circuit voltage. The use of a fixed acceptor LUMO level was adopted solely to enable an internally consistent comparison among the donor-modified molecules. Therefore, the calculated Voc, normalized Voc, and FF values should be interpreted as relative molecular-screening descriptors rather than absolute device-level photovoltaic parameters.

The normalized V_{oc} was calculated as:

$$v_{oc} = qV_{oc} / (nk_BT)$$

where q is the elementary charge, k_B is the Boltzmann constant, T is the temperature, and n is the ideality factor (33). For comparative evaluation, n = 1 was used. The fill factor (FF) was then estimated using the empirical relation (33).

$$FF = [v_{oc} - ln(v_{oc} + 0.72)] / (v_{oc} + 1)$$

The LUMO offset (ΔE_{LUMO}) was calculated to assess the energetic driving force for electron transfer from the investigated molecule to the reference acceptor (31).

$$\Delta E_{LUMO} = E_{LUMO}^{donor} - E_{LUMO}^{acceptor}$$

The E_b was estimated as the difference between the electronic HOMO–LUMO gap and the first TD-DFT excitation energy (34).

$$E_b = E_{H-L} - E_{opt}$$

where E_{opt} is the first vertical excitation energy obtained from TD-DFT calculations. Lower E_b values were considered favorable for exciton dissociation and charge separation. Because these E_b values were derived from isolated-molecule gas-phase calculations, dielectric screening, solid-state polarization, and donor–acceptor interfacial effects were not explicitly included. Therefore, the calculated E_b values may be overestimated relative to those in thin-film environments. In the present work, they are used as relative descriptors to compare donor-dependent trends within the same computational protocol.

Fragment-based orbital population analysis was performed using Multiwfn to quantitatively evaluate HOMO and LUMO localization (35). For each molecule, the optimized ground-state wavefunction was partitioned into three chemically meaningful fragments: the isoindigo acceptor core, the thiophene π-bridge, and the terminal donor units. Mulliken orbital composition analysis was then applied, and the fragment contributions were evaluated using the Mulliken "Total" term, which includes the coefficient contribution and overlap-related cross terms. Small negative contributions arising from overlap terms were considered negligible.

Global reactivity descriptors were estimated from the frontier-orbital energies using Koopmans' approximation (36). The ionization potential (IP) and electron affinity (EA) were calculated as:

$$IP \approx -E_{HOMO}$$
$$EA \approx -E_{LUMO}$$

These values were then used to calculate chemical hardness (η), chemical potential (μ), chemical softness (S), and electrophilicity index (ω) according to (36-39):

$$\eta = (IP - EA) / 2$$
$$\mu = -(IP + EA) / 2$$
$$S = 1 / 2\eta$$
$$\omega = \mu^2 / 2\eta$$

These descriptors were used to evaluate donor-dependent changes in electron-donating ability, electronic stability, polarizability, and electrophilic character.

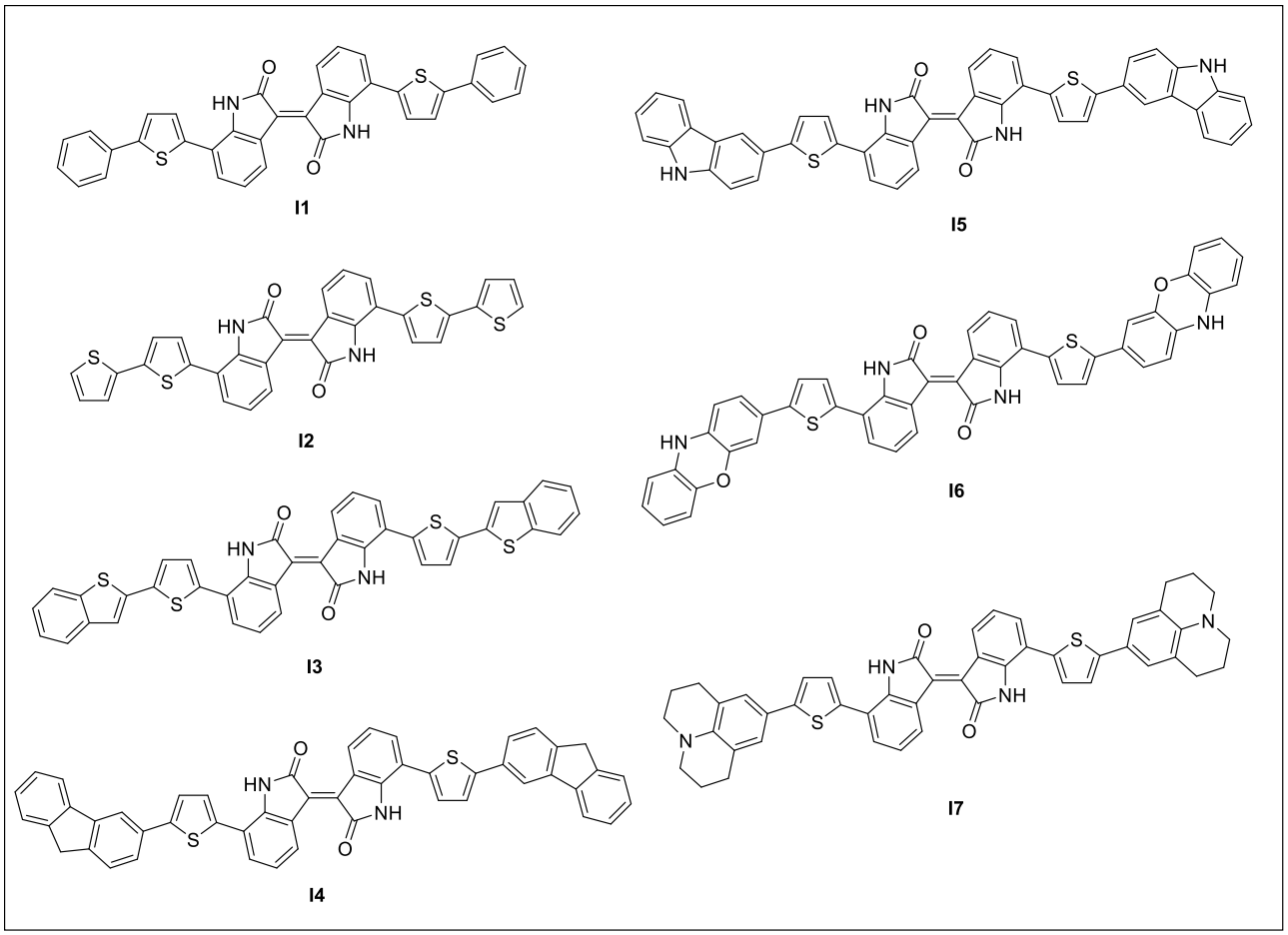

Figure 1: Structures of isoindigo-based D–A–D small molecules with different terminal donors.

3. RESULTS AND DISCUSSION

3.1. Benchmark Study

Prior to the systematic evaluation of the donor-modified molecular series, a benchmark study was performed to identify a consistent computational protocol for describing frontier molecular orbital energies of the reference isoindigo-based system (Table 1). The reference molecule was selected because experimental frontier orbital energies have been reported for a closely related isoindigo-containing donor–acceptor framework. Several exchange–correlation functionals and basis sets were tested, including B3LYP, CAM-B3LYP, B3PW91, HSEH1PBE, and ωB97XD in combination with Pople-type basis sets (40-46). The calculated HOMO and LUMO energies were compared with the available experimental values of −5.60 eV for the HOMO and −3.90 eV for the LUMO (47). Since the experimental values are typically derived from electrochemical measurements, whereas the calculated values correspond to gas-phase Kohn–Sham orbital energies, exact numerical agreement is not expected. Therefore, the benchmark was used to select a balanced and internally consistent level of theory for comparative screening, rather than to reproduce the absolute experimental orbital energies exactly.

The benchmark results showed that the calculated orbital energies were sensitive to both the functional and the basis set. In the B3LYP series, the inclusion of diffuse functions stabilized both the HOMO and LUMO levels. For example, changing the basis set from 6-31G to 6-31+G shifted the HOMO from −5.00 to −5.22 eV and the LUMO from −2.84 to −3.08 eV. A similar trend was observed for B3LYP/6-31+G(d,p), which produced HOMO and LUMO values of −5.16 and −2.99 eV, respectively. These results indicate that diffuse functions are important for improving the description of the low-lying virtual orbitals in this donor–acceptor framework.

Range-separated functionals showed larger deviations in the LUMO energy. CAM-B3LYP/6-31G(d,p) and ωB97XD/6-31G(d,p) produced considerably lower HOMO energies of −6.24 and −6.86 eV, respectively, while yielding relatively high LUMO energies of −1.65 and −1.14 eV. This resulted in an overestimated HOMO–LUMO separation compared with the expected electronic structure of the reference molecule. Therefore, although these functionals may be useful for certain charge-transfer excitations, they were not selected as the primary level of theory for the present comparative screening. Among the tested methods, B3PW91/6-31+G(d,p) provided a balanced description of the frontier molecular orbital energies while retaining a computationally affordable protocol for the complete molecular series. This level yielded HOMO and LUMO energies of −5.20 and −3.04 eV, respectively. We acknowledge that the calculated LUMO energy is higher than the experimental value, indicating that the absolute LUMO level is not quantitatively reproduced. However, similar discrepancies were observed for the other tested methods, and the range-separated functionals produced substantially larger HOMO–LUMO separations for the present reference system. B3PW91/6-31+G(d,p) was therefore selected not as an exact predictor of absolute experimental frontier orbital energies, but as a practical and internally consistent level of theory for comparing structurally related donor-modified molecules. The inclusion of both diffuse and polarization functions also provides a more complete basis-set description for the π-conjugated donor–acceptor framework. Accordingly, all geometry optimizations, frontier molecular orbital analyses, TD-DFT calculations, and derived OPV-related descriptors were evaluated using the same computational protocol so that the observed trends primarily reflect structural modification rather than methodological differences.

Table 1: Benchmark comparison of calculated HOMO and LUMO energies using different functional/basis set combinations for the reference molecule.

Functional	Basis set	HOMO (eV)	LUMO (eV)
B3LYP	6-31G	-5.00	-2.84
B3LYP	6-31+G	-5.22	-3.08
B3LYP	6-3G(d)	-4.90	-2.71
B3LYP	6-31G(d,p)	-4.91	-2.72
B3LYP	6-31+G(d,p)	-5.16	-2.99
CAM-B3LYP	6-31G(d,p)	-6.24	-1.65
B3PW91	6-31G(d,p)	-5.03	-2.83
B3PW91	6-31+G(d,p)	-5.20	-3.04
HSEH1PBE	6-31G(d,p)	-4.79	-3.00
wB97XD	6-31G(d,p)	-6.86	-1.14

3.2. Optimized Geometry and Structural Analysis

The optimized geometries of the donor-modified derivatives were further analyzed using selected bond-length and torsional parameters to understand how the donor units affect the π-conjugated backbone (Figure 2). Particular attention was given to the carbonyl bonds, C–N bonds, core–bridge C–C bonds, bridge C–S bonds, and bridge–donor C–C linkages, since these structural parameters are

directly related to conjugation, charge delocalization, and donor–acceptor electronic communication.

The calculated C=O bond lengths were highly consistent among the investigated molecules, with average values of 1.221–1.222 Å. This narrow variation indicates that the carbonyl-containing acceptor region preserves its local electronic structure upon donor modification. Similarly, the average C–N bond lengths remained nearly unchanged at approximately 1.380 Å for all derivatives, suggesting that the imide/lactam-type conjugated core is not significantly distorted by the terminal donor units (Table 2). Therefore, the major structural differences among the molecules arise primarily from the donor–π-bridge region rather than from the central acceptor core.

Table 2: Selected structural parameters of the optimized isoindigo-based donor–acceptor molecules **I1**–**I7** calculated at the B3PW91/6-31+G(d,p) level of theory.

Molecule	Donor	C=O avg.	C–N avg.	Core–bridge C–C	Bridge–donor C–C	Donor–bridge torsion
I1	Phenyl	1.221	1.380	1.459	1.465	28.0°
I2	Thiophene	1.221	1.380	1.458	1.447	21.4°
I3	Benzothiophene	1.221	1.380	1.458	1.446	16.4°
I4	Fluorene	1.222	1.380	1.458	1.464	28.6°
I5	Carbazole	1.222	1.380	1.458	1.464	29.6°
I6	Phenoxazine	1.222	1.380	1.458	1.461	27.5°
I7	Julolidine	1.222	1.380	1.456	1.460	25.5°

The core–bridge C–C bond lengths were also very similar, ranging from 1.456 to 1.459 Å. These values indicate that the connection between the central conjugated framework and the thiophene bridge retains partial π-conjugated character across the entire series. The bridge C–S bonds were calculated in the range of 1.741–1.743 Å, which is typical for thiophene-containing π-conjugated systems and confirms that the thiophene bridge remains structurally stable after donor substitution. More pronounced differences were observed for the bridge–donor C–C linkages. The phenyl-substituted derivative **I1** displayed a bridge–donor bond length of 1.465 Å, indicating a relatively pronounced single-bond character between the phenyl donor and the thiophene bridge. In contrast, the thiophene and benzothiophene derivatives (**I2** and **I3**, respectively) showed shorter bridge–donor C–C bonds of 1.447 and 1.446 Å, respectively. These shorter bond lengths suggest enhanced π-conjugation and stronger electronic communication between the donor unit and the conjugated backbone. For the thiophene derivative **I2**, the bridge–donor C–C bond was similarly short at 1.447 Å, while the donor–bridge torsion angle was slightly larger than that of benzothiophene. This indicates efficient but somewhat less extended π-conjugation compared with the benzothiophene analogue. This structural feature is consistent with its strong optical response and high LHE value, supporting thiophene as a favorable donor unit for maintaining electronic communication without causing excessive HOMO destabilization. The benzothiophene derivative **I3** showed the most planar donor–bridge arrangement, with a representative torsional deviation of approximately 16.4°. This greater planarity, together with the shortest bridge–donor C–C linkage, supports more effective π-electron delocalization along the molecular backbone.

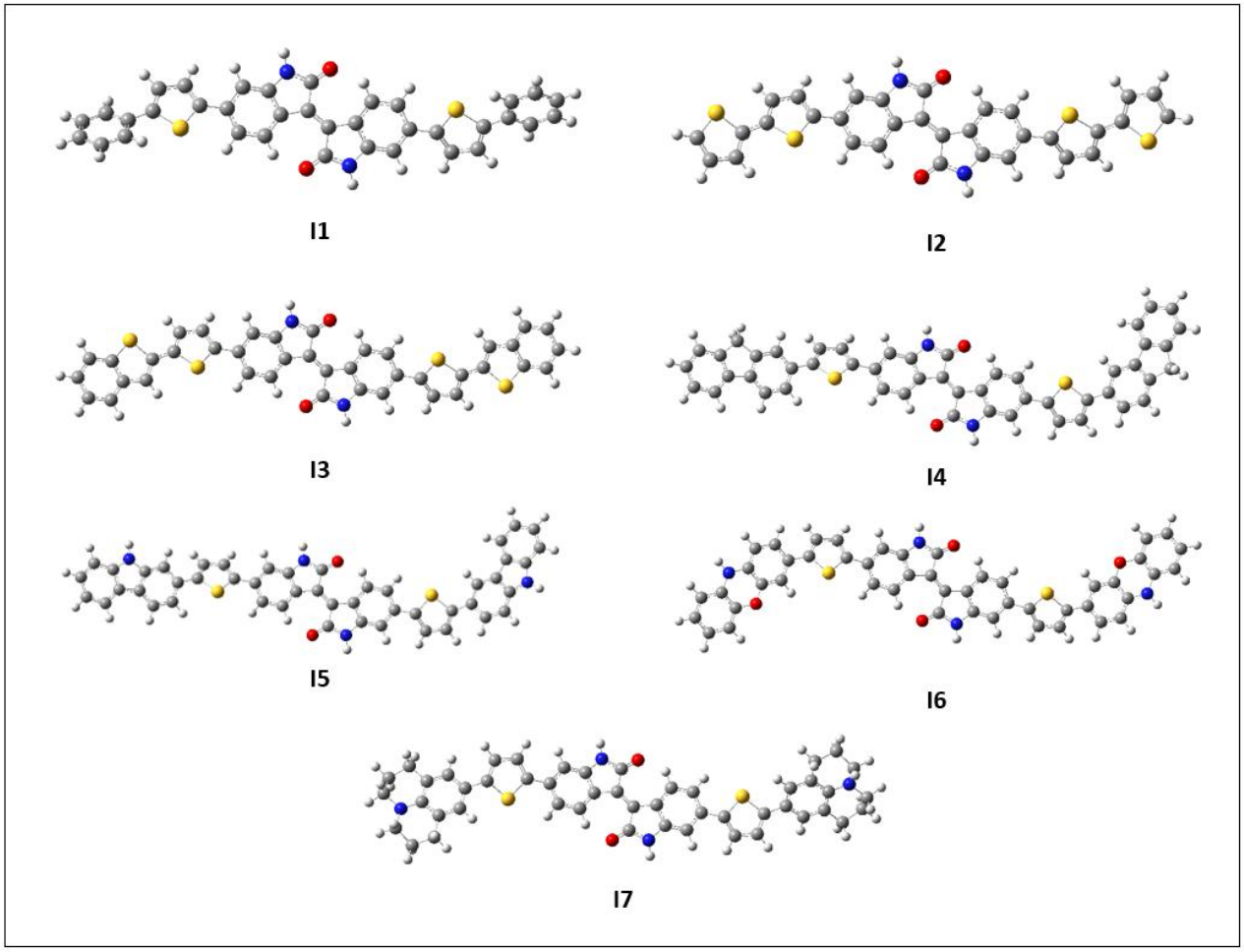

Figure 2: Optimized molecular geometries of the donor-modified conjugated molecules **I1–I7** calculated at the B3PW91/6-31+G(d,p) level of theory.

The fluorene and carbazole derivatives (**I4** and **I5**, respectively) exhibited longer bridge–donor C–C bonds of approximately 1.464 Å and larger torsional deviations of 28.6° and 29.6°, respectively. These values suggest that the donor units are more twisted with respect to the thiophene bridge, which may reduce orbital overlap between the donor and the π-conjugated backbone. Nevertheless, both derivatives retain favorable optical and OPV-related descriptors, indicating that their rigid aromatic frameworks still support sufficient conjugation for OPV-relevant electronic transitions.

The phenoxazine derivative **I6** showed a bridge–donor C–C bond length of 1.461 Å and a donor–bridge torsion of approximately 27.5°. Although the structural conjugation is not as strong as in the thiophene and benzothiophene derivatives, the stronger electron-donating character of phenoxazine contributes to a significant bathochromic shift. However, this red-shifted absorption is accompanied by HOMO destabilization and a reduction in V_{oc}, indicating that electronic donor strength rather than enhanced backbone planarity is the dominant factor governing this behavior.

The julolidine derivative **I7** also showed a relatively long bridge–donor C–C bond of 1.460 Å, with a torsional deviation of approximately 25.5°. Despite not having the shortest donor–bridge bond, julolidine produced the most red-shifted absorption and the narrowest HOMO–LUMO gap. This behavior can be attributed to its strong electron-donating character and increased HOMO destabilization. However, the same effect leads to the lowest estimated V_{oc} and a reduced FF, demonstrating that excessive donor strength can be detrimental to the overall photovoltaic balance.

Overall, the structural analysis demonstrates that the central acceptor core remains geometrically stable across the molecular series, while the donor–bridge region controls the extent of conjugation and electronic communication. Shorter bridge–donor C–C bonds and lower torsional deviations, as observed for the thiophene and benzothiophene derivatives, favor improved π-delocalization and stronger optical transitions. In contrast, stronger donor units such as phenoxazine and julolidine mainly tune the electronic structure through HOMO destabilization, leading to red-shifted absorption but also reduced voltage retention. It should also be noted that the present structural analysis is based on isolated molecular geometries. Intermolecular π–π stacking, side-chain effects, solid-state packing, crystallinity, blend morphology, and donor–acceptor interfacial organization were not explicitly modeled. These factors are critical determinants of actual OPV device performance and should be addressed in future studies using aggregate models, molecular

dynamics, periodic calculations, or experimental thin-film characterization. Therefore, the present results should be interpreted as molecular-level design guidelines rather than direct device-performance predictions.

3.3. Frontier Molecular Orbital Distribution

The spatial distributions of the HOMO and LUMO orbitals were examined to further elucidate the donor–acceptor electronic communication in molecules **I1**–**I7**. The HOMO and LUMO plots are presented in Figure 3. In general, the HOMOs are mainly distributed over the electron-rich donor units and the π-conjugated bridge, whereas the LUMOs are predominantly localized on the electron-deficient central acceptor core. However, the donor units also exert a measurable effect on the LUMO, as reflected by the LUMO energy variation across the series. Therefore, the orbital distributions should be interpreted as donor-modulated donor–acceptor electronic structures rather than as fully separated frontier orbitals. This spatial distribution supports intramolecular charge-transfer character from the donor-rich segments toward the isoindigo acceptor region upon electronic excitation. For **I1**, the HOMO is distributed mainly along the conjugated backbone with relatively limited contribution from the terminal phenyl groups. The LUMO is more localized on the central acceptor-containing region, showing that phenyl acts as a weaker donor unit. This is consistent with the deeper HOMO level and larger HOMO–LUMO gap observed for **I1**. In the thiophene derivative I2, the HOMO distribution extends more effectively over the terminal thiophene donors and the π-bridge, indicating stronger conjugation compared with **I1**. The LUMO remains largely concentrated on the central acceptor core. This donor-to-acceptor orbital separation supports the improved optical response, higher f, and enhanced LHE of **I2**.

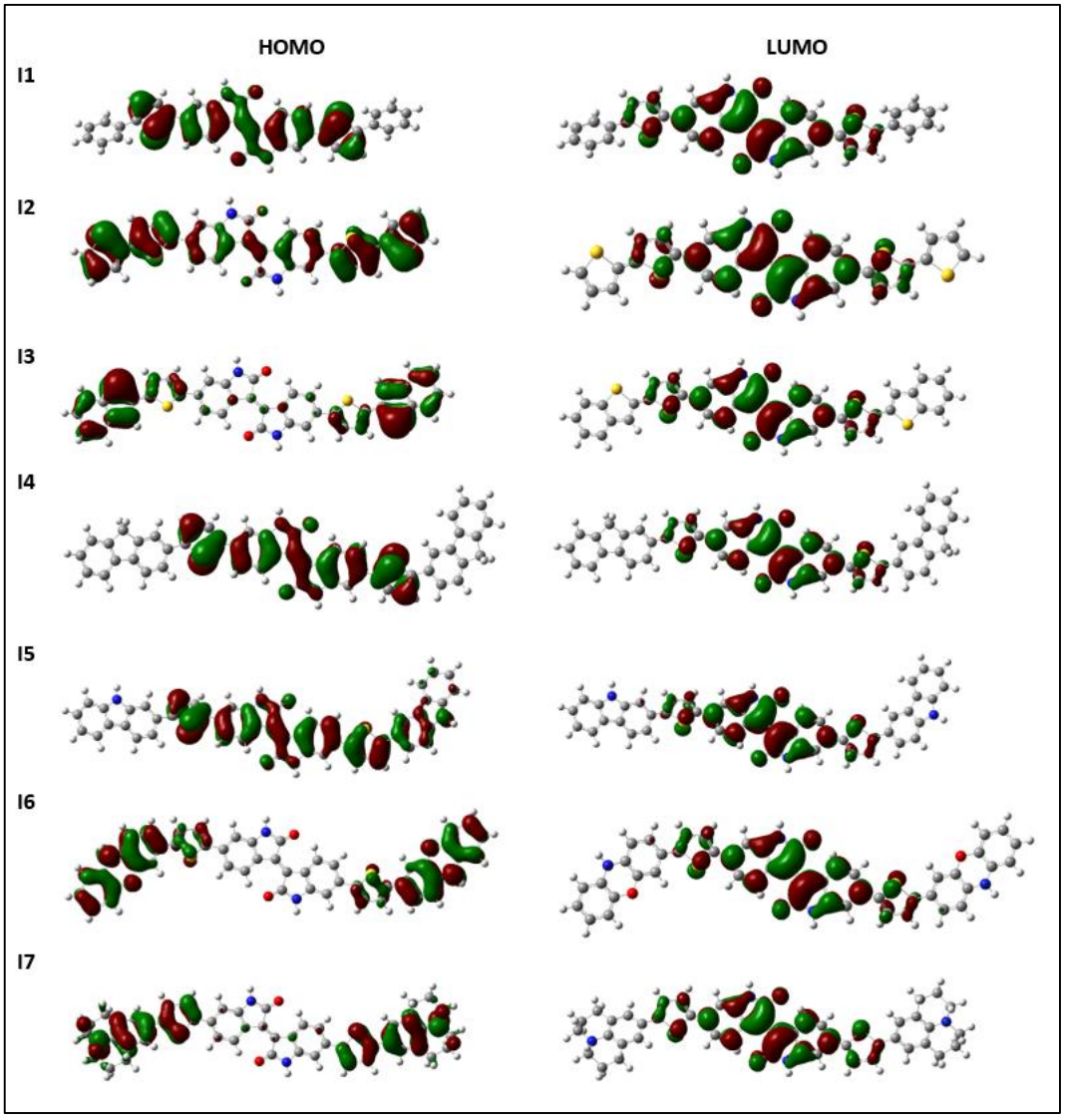

Figure 3: HOMO and LUMO orbital distributions of the donor-modified molecules I1–I7 calculated at the B3PW91/6-31+G(d,p) level.

For **I3**, the HOMO is well delocalized over the benzothiophene donor units and the conjugated bridge, while the LUMO is mainly localized on the acceptor region. This balanced HOMO delocalization and LUMO localization suggests efficient intramolecular charge transfer without excessive HOMO destabilization. This feature agrees well with the favorable photovoltaic profile of **I3**, including its high f, high LHE, low E_b, and high estimated V_{oc}. The fluorene derivative **I4** also shows HOMO distribution

over the donor-containing conjugated framework, although the terminal donor contribution appears somewhat more spatially separated due to the rigid fluorene units. The LUMO remains centered on the acceptor core. This indicates that **I4** maintains donor–acceptor electronic communication while preserving a relatively balanced frontier orbital alignment. For the carbazole derivative I5, the HOMO shows a clear contribution from the carbazole donor units and the π-conjugated backbone. The LUMO is again mainly localized on the central acceptor moiety. The increased donor contribution in the HOMO is consistent with the upward shift of the HOMO energy and the reduced HOMO–LUMO gap compared with weaker donor derivatives. However, this stronger donor effect also contributes to a moderate decrease in the estimated V_{oc}. In **I6**, the HOMO is strongly distributed over the phenoxazine donor units, reflecting the pronounced electron-donating character of this donor. In contrast, the LUMO remains predominantly localized on the acceptor core. This stronger spatial separation between HOMO and LUMO supports more pronounced intramolecular charge-transfer character and explains the bathochromic shift observed for **I6**. However, the strong HOMO destabilization also leads to a lower V_{oc}.

The julolidine derivative **I7** exhibits the strongest donor contribution in the HOMO among the series. The HOMO is mainly localized over the julolidine donor regions and adjacent conjugated segments, while the LUMO remains concentrated on the central acceptor framework. This pronounced donor–acceptor orbital separation is consistent with the smallest energy gap and the most red-shifted absorption maximum. Nevertheless, the excessive HOMO elevation in **I7** results in the lowest V_{oc} and reduced overall photovoltaic balance. Overall, the orbital distribution analysis confirms that donor modification mainly affects the HOMO distribution, while the LUMO is largely governed by the central acceptor core. This explains why the HOMO energies vary more significantly than the LUMO energies across the molecular series. Moderate donors such as thiophene, benzothiophene, and fluorene provide efficient HOMO delocalization while maintaining suitable frontier orbital alignment. In contrast, stronger donors such as phenoxazine and julolidine enhance charge-transfer character and red-shifted absorption, but at the cost of HOMO destabilization and voltage loss.

3.4. Frontier Molecular Orbital Energies

The frontier molecular orbital energies of the investigated donor-modified molecules, labeled as I1–I7, were calculated at the B3PW91/6-31+G(d,p) level. The HOMO and LUMO energies are presented in Figure 4 in electron volts. The results clearly show that the electronic structure of the molecules depends strongly on the terminal donor unit.

The phenyl-substituted molecule **I1** exhibited a HOMO energy of −5.53 eV and a LUMO energy of −3.21 eV. Among the investigated series, **I1** exhibited the deepest HOMO level, indicating the weakest electron-donating contribution from the phenyl group. This deeper HOMO level is beneficial for maintaining a relatively high V_{oc}, but the weaker donor character also leads to a larger electronic gap compared with the more electron-rich derivatives. The thiophene-substituted molecule **I2** showed a HOMO energy of −5.46 eV and a LUMO energy of −3.24 eV. Compared with **I1**, the HOMO level of **I2** is slightly destabilized, reflecting the stronger electron-donating and π-conjugating ability of thiophene. At the same time, the LUMO level is slightly stabilized relative to **I1**. This combination suggests improved donor–acceptor electronic communication while still preserving a sufficiently deep HOMO level for favorable voltage retention. The benzothiophene-substituted molecule **I3** displayed a HOMO energy of −5.52 eV and the lowest LUMO energy of the series, −3.31 eV. The deep HOMO level of **I3** indicates that benzothiophene does not excessively destabilize the donor framework, while its more stabilized LUMO suggests enhanced electron-accepting character and stronger electronic interaction with the acceptor core.

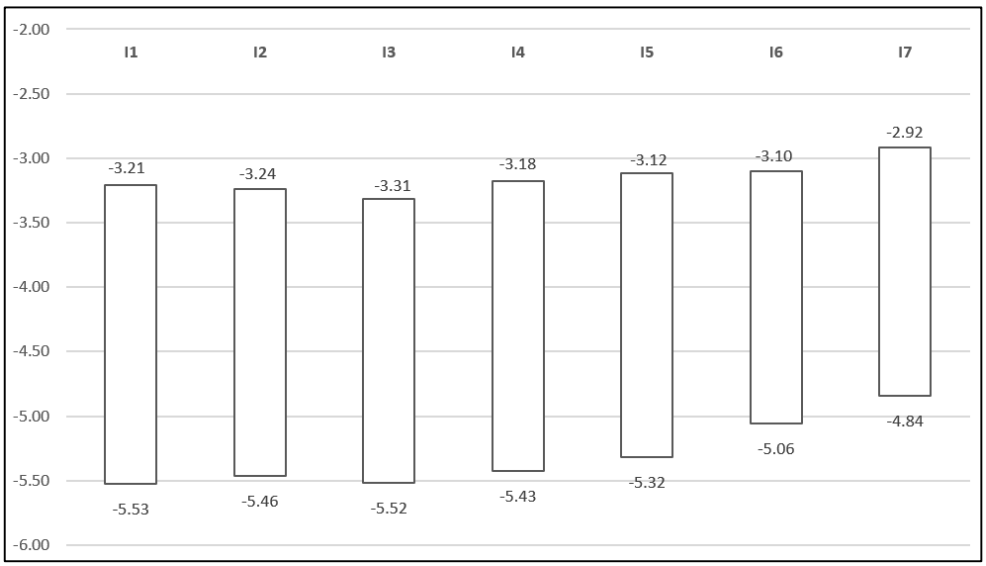

Figure 4: Frontier molecular orbital energy levels of isoindigo-based donor–acceptor molecules **I1–I7** calculated at the B3PW91/6-31+G(d,p) level of theory.

This makes **I3** one of the most electronically balanced molecules in the series. The combination of a deep HOMO and low LUMO is also consistent with its favorable optical and photovoltaic descriptors. The fluorene-substituted molecule **I4** had HOMO and LUMO energies of −5.43 eV and −3.18 eV, respectively. The HOMO level is slightly higher than those of **I1**–**I3**, indicating moderate donor strength. However, the LUMO is less stabilized than in **I2** and **I3**. This suggests that fluorene contributes to HOMO modulation more than to LUMO stabilization. Therefore, **I4** can be considered a moderate donor-containing system that maintains acceptable frontier orbital alignment without excessive narrowing of the electronic gap. The carbazole-substituted molecule **I5** showed a HOMO energy of −5.32 eV and a LUMO energy of **−**3.12 eV. The upward shift of the HOMO compared with **I1**–**I4** confirms the stronger electron-donating character of carbazole. This HOMO destabilization contributes to a reduced HOMO–LUMO gap and can promote a red shift in absorption. However, the higher HOMO level may also lead to a decrease in the estimated V_{oc}. Thus, **I5** represents a transition point between moderate donor systems and stronger donor-substituted derivatives. The phenoxazine-substituted molecule **I6** exhibited a HOMO energy of −5.06 eV and a LUMO energy of −3.10 eV. The HOMO level is considerably higher than those of **I1**–**I5**, indicating the strong electron-donating nature of phenoxazine. This significant HOMO destabilization leads to a narrower HOMO–LUMO gap and supports the pronounced bathochromic shift observed in the optical absorption data. However, this electronic advantage is accompanied by a reduction in the estimated V_{oc}, since the elevated HOMO level decreases the energetic driving force for high V_{oc}. The julolidine-substituted molecule **I7** showed the highest HOMO level, −4.84 eV, and the highest LUMO level, −2.92 eV, among the series. This result reflects the strongest donor effect in the investigated molecules. The highly destabilized HOMO level of **I7** leads to the smallest HOMO–LUMO gap and the most red-shifted absorption behavior. However, the excessive HOMO elevation is unfavorable for maintaining a high estimated photovoltaic voltage. Therefore, although julolidine is effective in extending absorption toward longer wavelengths, it appears less suitable for achieving a balanced OPV-related descriptor profile.

Overall, the HOMO energies follow the trend I1 < I3 ≈ I2 < I4 < I5 < I6 < I7, in order of increasing energy. This trend confirms that stronger donor units progressively destabilize the HOMO level. In contrast to the HOMO levels, the LUMO energies vary within a relatively narrower range, from −3.31 to −2.92 eV. This indicates that the LUMO is still largely governed by the electron-deficient isoindigo acceptor core, but it is also measurably modulated by the terminal donor units. Therefore, the reduction in the HOMO–LUMO gap across the series is mainly caused by HOMO destabilization, while donor-induced LUMO shifts also contribute to the final frontier orbital alignment.

These results indicate that the donor-dependent electronic modulation is mainly governed by HOMO destabilization rather than LUMO variation. Moderate donors such as thiophene, benzothiophene, and fluorene provide balanced frontier orbital alignments, whereas stronger donors such as phenoxazine and julolidine excessively raise the HOMO level. Consequently, although strong donors reduce the HOMO–LUMO gap and promote red-shifted absorption, they may also compromise the V_{oc}. Among the investigated molecules, **I3**, containing benzothiophene, appears to be the most promising derivative in terms of frontier orbital alignment.

3.5. Orbital Population Analysis

To quantitatively support the frontier-orbital localization analysis, a fragment-based Mulliken orbital composition analysis was performed using Multiwfn. Each molecule was divided into three chemically meaningful fragments: the isoindigo acceptor core, the thiophene π-bridge, and the terminal donor units. The calculated fragment contributions to the HOMO and LUMO are summarized in Table 3.

The results show that the LUMO is consistently dominated by the isoindigo acceptor core for all investigated molecules. The core contribution to the LUMO remained within a narrow range of 86.29–87.05%, while the thiophene bridge contributes only 11.39–12.07% and the contribution of the terminal donors is minor, ranging from 0.90 to 2.07%. These results quantitatively confirm that the LUMO is primarily acceptor-centered across the I1–I7 series.

In contrast, the HOMO distribution is strongly affected by the nature of the terminal donor unit. For I1 and I4, the HOMO is mainly delocalized over the thiophene bridge and isoindigo core, with bridge/core contributions of 54.88/45.21% and 52.70/46.68%, respectively. For I2 and I5, the donor contribution increases to 47.46% and 11.99%, respectively, indicating donor-dependent modulation of the occupied orbital distribution. In I3, I6, and I7, the HOMO becomes predominantly localized on the terminal donor units, with donor contributions of 86.57%, 87.74%, and 73.77%, respectively.

Overall, the fragment-based orbital composition analysis demonstrates that terminal donor modification mainly modulates the HOMO distribution, whereas the LUMO remains largely localized on the isoindigo acceptor core. This donor-sensitive HOMO localization combined with an acceptor-centered LUMO supports the donor-to-acceptor intramolecular charge-transfer character of the lowest-energy electronic transition.

Table 3: Fragment-based Mulliken orbital composition analysis of the HOMO and LUMO for I1–I7. Each molecule was partitioned into three fragments: the isoindigo acceptor core, thiophene π-bridge, and terminal donor units. Values represent percentage contributions obtained from the Mulliken "Total" term in Multiwfn. Small negative contributions arising from overlap terms were considered negligible.

Molecule	HOMO core (%)	HOMO bridge (%)	HOMO donor (%)	LUMO core (%)	LUMO bridge (%)	LUMO donor (%)	Dominant orbital character
I1	45.21	54.88	0.00	87.04	12.07	0.90	HOMO bridge/core delocalized; LUMO core-centered
I2	17.40	35.14	47.46	86.93	11.62	1.46	HOMO donor/bridge; LUMO core-centered
I3	5.07	8.36	86.57	86.29	11.64	2.07	HOMO donor-centered; LUMO core-centered
I4	46.68	52.70	0.62	86.84	11.41	1.75	HOMO bridge/core delocalized; LUMO core-centered
I5	45.84	42.17	11.99	87.05	11.42	1.53	HOMO core/bridge delocalized; LUMO core-centered
I6	1.70	10.56	87.74	86.68	11.39	1.93	HOMO donor-centered; LUMO core-centered
I7	3.74	22.49	73.77	86.52	11.85	1.63	HOMO donor-centered; LUMO core-centered

3.6. Low-Energy Electronic Transitions and ICT Character

To further support the intramolecular charge-transfer interpretation inferred from the frontier molecular orbital distributions, the dominant low-energy electronic transitions were examined using the TD-DFT results. As summarized in Table 4, the S1 transitions of all derivatives are dominated by HOMO→LUMO excitations, with contributions of approximately 98.6–99.6%. Because the HOMO is mainly distributed over the terminal donor units and π-conjugated bridge, whereas the LUMO is largely localized on the isoindigo acceptor core, these low-energy transitions can be assigned to donor-to-acceptor intramolecular charge-transfer transitions. These results indicate that terminal donor modification strongly influences the ICT character by modulating the HOMO level while the LUMO remains mainly governed by the central acceptor unit.

Table 4: Dominant low-energy electronic transitions of isoindigo-based donor–acceptor molecules calculated at the TD-B3PW91/6-31+G(d,p) level.

Molecule	Excited state	Dominant transition	Coefficient	Contribution (%)	ICT assignment
I1	S1	HOMO → LUMO	0.70221	98.6	Moderate donor-to-acceptor ICT
I2	S1	HOMO → LUMO	0.70356	99.0	Clear donor-to-acceptor ICT
I3	S1	HOMO → LUMO	0.70260	98.7	Balanced donor-to-acceptor ICT
I4	S1	HOMO → LUMO	0.70200	98.6	Moderate/balanced ICT
I5	S1	HOMO → LUMO	0.70213	98.6	Enhanced donor-to-acceptor ICT
I6	S1	HOMO → LUMO	0.70435	99.2	Pronounced ICT with red-shifted absorption
I7	S1	HOMO → LUMO	0.70580	99.6	Strong ICT but excessive HOMO destabilization

Among the investigated molecules, **I3** exhibits a particularly balanced ICT profile, combining strong HOMO→LUMO transition character with the highest f and a relatively deep HOMO level. In contrast, **I6** and **I7** show more pronounced low-energy ICT transitions and stronger bathochromic shifts, but these are accompanied by excessive HOMO destabilization and reduced voltage-related descriptors. Therefore, the TD-DFT transition analysis supports the conclusion that moderate donor strength is more favorable than excessive electron donation for a balanced OPV-related descriptor profile.

3.7. OPV-Related Molecular Descriptors

The photovoltaic properties of the donor-modified molecules **I1–I7** were evaluated using key descriptors including the maximum absorption wavelength, oscillator strength, light-harvesting efficiency, estimated open-circuit voltage, normalized open-circuit voltage, fill factor, optical gap, LUMO offset, and E_b (Table 5). These parameters provide insight into the balance between light absorption, charge separation, and voltage generation in the investigated OPV candidates.

The phenyl-substituted molecule **I1** exhibited an absorption maximum at 639.28 nm, with an f of 1.39 and a LHE of 0.96. Its calculated electronic gap was 2.32 eV, while the optical gap was 1.94 eV, giving an E_b of 0.38 eV. **I1** also showed the highest estimated V_{oc} in the series, 1.28 V, together with a normalized V_{oc} of 49.33 and a fill factor of 0.90. These results indicate that the phenyl donor preserves a deep HOMO level and therefore supports high voltage output. However, compared with more π-extended donors, its absorption is relatively blue-shifted. The thiophene-substituted molecule **I2** showed a red-shifted absorption maximum at 669.47 nm, with a higher f of 1.51 and an improved LHE value of 0.97. The HOMO–LUMO gap decreased to 2.22 eV, and the optical gap was calculated as 1.85 eV. Its E_b was 0.37 eV, slightly lower than that of **I1**. The estimated V_{oc} of **I2** was 1.21 V, with a normalized V_{oc} of 46.86 and a fill factor of 0.90. This profile suggests that thiophene improves the optical response while maintaining a sufficiently high voltage, making **I2** one of the balanced candidates in the series.

Table 5: Electronic, optical, and photovoltaic descriptors of the isoindigo-based donor–acceptor molecules **I1–I7** calculated at the B3PW91/6-31+G(d,p) level.

	HOMO (eV)	LUMO (eV)	λ_{max} (nm)	f	V_{oc} (V)	v_{oc}	FF	LHE *	E_{H-L} (eV)	ΔLUMO (eV)	E_{opt} (eV)	E_b (eV)
I1	-5.53	-3.21	639	1.39	1.28	49.33	0.90	0.96	2.32	0.74	1.94	0.38
I2	-5.46	-3.24	669	1.51	1.21	46.86	0.90	0.97	2.22	0.71	1.85	0.37
I3	-5.52	-3.31	672	1.67	1.27	48.97	0.90	0.98	2.21	0.64	1.84	0.36
I4	-5.43	-3.18	663	1.60	1.18	45.37	0.90	0.97	2.25	0.77	1.87	0.38
I5	-5.32	-3.12	684	1.58	1.07	41.25	0.89	0.97	2.20	0.83	1.81	0.39
I6	-5.06	-3.10	803	1.14	0.81	31.17	0.86	0.93	1.96	0.85	1.54	0.41
I7*	-4.84	-2.92	837	1.43	0.59	22.90	0.83	0.96	1.93	1.03	1.48	0.45

*LHE values were calculated from the oscillator strength of the main low-energy absorption maximum using the same transition-selection criterion for all derivatives. For **I7**, the visible-region oscillator strength was additionally considered in the discussion because its strongest absorption is located near the near-infrared edge of the conventional visible range.

The benzothiophene-substituted molecule **I3** displayed one of the most favorable OPV-related descriptor profiles. It showed an absorption maximum at 672.55 nm and the highest f of the series, 1.67. Accordingly, **I3** also exhibited the highest LHE value, 0.98, indicating a high calculated light-harvesting efficiency. Its HOMO–LUMO gap was 2.21 eV, and the optical gap was 1.84 eV, resulting in the lowest E_b of 0.36 eV. In addition, **I3** maintained a high estimated Voc of 1.27 V, a normalized V_{oc} of 48.97, and a fill factor of 0.90. The combination of strong absorption, high LHE, low E_b, suitable ΔLUMO, and high estimated V_{oc} identifies I3 as the most favorable molecular-level screening candidate among the investigated derivatives.

The fluorene-substituted molecule **I4** showed an absorption maximum at 663.47 nm, with an f of 1.60 and an LHE value of 0.97. Its electronic gap was 2.25 eV, while the optical gap was 1.87 eV, giving an E_b of 0.38 eV. The estimated V_{oc} was 1.18 V, with a normalized V_{oc} of 45.37 and a fill factor of 0.90. Although the voltage is slightly lower than those of **I1** and **I3**, **I4** still shows a well-balanced OPV profile due to its strong oscillator strength, high LHE, and a favorable estimated V_{oc}. The carbazole-substituted molecule **I5** exhibited a further red-shifted absorption maximum at 684.54 nm. Its f was 1.58, and the LHE value remained high at 0.97. The electronic gap was 2.20 eV, and the optical gap was 1.81 eV, giving an E_b of 0.39 eV. However, the estimated V_{oc} decreased to 1.07 V, with a normalized V_{oc} of 41.25 and a fill factor of 0.89. These results show that carbazole promotes a red shift in absorption while still preserving good light-harvesting ability, but its stronger donor character results in a lower estimated V_{oc}.

The phenoxazine-substituted molecule **I6** showed a pronounced bathochromic shift, with an absorption maximum at 803.10 nm. This indicates that phenoxazine strongly narrows the optical transition energy and extends absorption toward the near-infrared region. The oscillator strength was 1.14 and the calculated LHE was 0.93, both lower than the corresponding values for I2–I5. The electronic gap decreased to 1.96 eV, and the optical gap was 1.54 eV, yielding an E_b of 0.41 eV. However, the estimated V_{oc} dropped significantly to 0.81 V, with a normalized V_{oc} of 31.17 and a fill factor of 0.86. Therefore, **I6** is effective for red-shifted absorption, but its high HOMO level leads to a substantial decrease in the estimated V_{oc}.

The julolidine-substituted molecule **I7** exhibited the most red-shifted absorption maximum at 837.87 nm and the smallest electronic and optical gaps of 1.93 and 1.48 eV, respectively. Based on the oscillator

strength of the main low-energy transition (f = 1.43), the corresponding LHE value remains high at approximately 0.96. However, because this transition is located near the near-infrared edge of the conventional visible region, the visible-region oscillator strength was additionally considered. Within the 400–800 nm range, the oscillator strength decreased to 0.56, corresponding to a visible-region LHE of 0.73. Therefore, although julolidine strongly extends absorption toward longer wavelengths, its excessive donor strength causes severe HOMO destabilization, reduced voltage output, and less favorable overall OPV balance.

Overall, the photovoltaic descriptors reveal a clear trade-off between red-shifted absorption and voltage preservation. Stronger donor units such as phenoxazine and julolidine decrease the electronic and optical gaps and shift the absorption maximum toward longer wavelengths. However, this effect is accompanied by a significant decrease in Voc, normalized Voc, and FF, and in the case of julolidine, by a reduced visible-region oscillator strength and visible-region LHE. In contrast, moderate donor units such as thiophene, benzothiophene, and fluorene provide a more favorable balance between absorption strength and voltage output. Among all investigated molecules, **I3** bearing benzothiophene appears to be the best OPV candidate because it combines the highest oscillator strength, the highest LHE, the lowest E_b, and a high estimated V_{oc}. **I2** bearing thiophene and **I4** bearing fluorene also show promising and balanced photovoltaic properties. Therefore, the overall descriptor-based OPV screening trend can be proposed as: **I3** > **I2** ≈ **I4** > **I1** ≈ **I5** > **I6** > **I7**. These findings indicate that the best photovoltaic performance is not obtained simply by maximizing the bathochromic shift, but by balancing absorption strength, exciton dissociation ability, and voltage preservation. In this respect, benzothiophene, thiophene, and fluorene are more suitable donor units than stronger donors such as phenoxazine and julolidine.

The E_b and LUMO offset were further evaluated to assess the potential of the investigated molecules for exciton dissociation and electron transfer. In organic photovoltaic materials, efficient charge generation requires not only strong light absorption but also effective separation of the photogenerated electron–hole pair. Therefore, low E_b and a suitable energetic offset between the donor LUMO and the acceptor LUMO are important criteria for evaluating OPV candidates.

The E_b, calculated as the difference between the electronic HOMO–LUMO gap and the optical transition energy, varied from 0.36 to 0.45 eV across the molecular series. The lowest value was obtained for **I3** bearing benzothiophene, with an E_b of 0.36 eV, followed by **I2** bearing thiophene with 0.37 eV. These relatively low values suggest that the photogenerated excitons in **I2** and **I3** may dissociate more readily than those in the other derivatives. This result is consistent with their strong oscillator strengths, high light-harvesting efficiencies, and balanced frontier molecular orbital alignments. The phenyl derivative **I1** and fluorene derivative **I4** both showed E_b values of 0.38 eV, indicating moderate exciton binding. The carbazole derivative **I5** gave a slightly higher E_b value of 0.39 eV. Although **I5** exhibits red-shifted absorption and high LHE, the increase in E_b suggests that the stronger donor character of carbazole does not necessarily improve exciton separation. This confirms that bathochromic absorption alone is not sufficient for achieving a balanced OPV-related descriptor profile. Higher Eb values were observed for I6 (phenoxazine) and I7 (julolidine), with values of 0.41 and 0.45 eV, respectively. These molecules show the most red-shifted absorption maxima and the smallest optical gaps; however, their higher exciton binding energies indicate stronger electron–hole attraction in the excited state. This may hinder charge separation to a greater extent, especially for **I7**, which also exhibits the lowest V_{oc}, FF, and LHE values in the series. Therefore, the E_b trend shows that excessive donor strength can narrow the optical gap but may also reduce the overall photovoltaic balance.

The LUMO offset, ΔLUMO, was also considered as an indicator of the energetic driving force for electron transfer from the donor molecule to the acceptor. In the present series, ΔLUMO values ranged from 0.64 to 1.03 eV. All molecules exhibited positive and sufficiently large LUMO offsets, suggesting that electron transfer to the acceptor is energetically feasible. However, very large offsets may lead to unnecessary energetic losses and may negatively affect the overall voltage balance. Among the investigated molecules, **I3** showed the smallest ΔLUMO value of 0.64 eV, together with the lowest E_b value of 0.36 eV. This combination appears favorable within the present screening framework because it indicates that **I3** provides a sufficient calculated driving force for electron transfer while minimizing excessive energy loss. Similarly, **I2** thiophene exhibited a suitable ΔLUMO value of 0.71 eV and a low E_b value of 0.37 eV, supporting its balanced charge-separation potential. In contrast, **I7** exhibited the highest ΔLUMO value of 1.03 eV and the highest E_b value of 0.45 eV. Although this large LUMO offset may provide a strong thermodynamic driving force for electron transfer, it may also introduce excessive energetic loss. Together with its low V_{oc} and reduced visible-region LHE, this suggests that **I7** is less favorable for efficient OPV performance despite its strong bathochromic absorption.

Overall, the combined E_b and ΔLUMO analysis confirms that the most promising candidates are not simply those with the most red-shifted absorption, but those that provide an optimal balance between exciton dissociation, electron-transfer driving force, and voltage retention. In this respect, **I3** bearing benzothiophene appears to be the most favorable molecule at the molecular screening level, followed by **I2** bearing thiophene and **I4** bearing fluorene. These derivatives combine relatively low exciton binding energies with suitable LUMO offsets and favorable OPV-related descriptors. Nevertheless, these descriptors are derived from simplified molecular models and do not include dielectric

screening, explicit donor–acceptor interfaces, morphology, charge mobility, or recombination processes. Therefore, the ranking proposed here should be regarded as a guide for future computational and experimental screening rather than a direct prediction of device efficiency.

3.8. Global Reactivity Descriptors

To further evaluate the electronic characteristics of the donor-modified molecules, global reactivity descriptors were estimated from the frontier-orbital energies using Koopmans' approximation (Table 6). The ionization potential (IP) and electron affinity (EA) were calculated from HOMO and LUMO energies. These values were then used to derive chemical hardness (η), chemical potential (μ), chemical softness (S), and electrophilicity index (ω). It should be noted that Koopmans' approximation neglects orbital relaxation and geometry relaxation effects associated with charged states. Therefore, the IP and EA values reported here should not be interpreted as quantitatively exact ionization and electron-attachment energies. Instead, they are used as internally consistent qualitative descriptors for comparing donor-dependent electronic trends. More rigorous ΔSCF calculations would be required for quantitatively reliable vertical or adiabatic IP and EA values.

The calculated ionization potentials varied from 5.53 eV for **I1** to 4.84 eV for **I7**. This gradual decrease in IP indicates that stronger donor units facilitate electron removal by destabilizing the HOMO level. Among the series, **I1** and **I3** showed relatively high IP values of 5.53 and 5.52 eV, respectively, suggesting greater oxidative stability and deeper HOMO levels. In contrast, **I6** and **I7** exhibited lower IP values of 5.06 and 4.84 eV, confirming their stronger electron-donating character. The estimated electron affinities ranged from 2.92–3.31 eV. The highest EA was obtained for **I3** with a value of 3.31 eV, indicating the strongest estimated electron-accepting tendency among the investigated derivatives. This result is consistent with the more stabilized LUMO level of **I3** and supports its balanced donor–acceptor electronic structure. **I2** also showed a relatively high EA value of 3.24 eV, whereas **I7** gave the lowest EA value of 2.92 eV, reflecting its destabilized LUMO level and strong donor-induced electronic perturbation.

Chemical hardness, η, decreased from 1.16 eV for **I1** to 0.96 eV for **I7**. This decrease indicates that the electronic structure becomes softer and more polarizable as the donor strength increases. The corresponding softness values increased from 0.43 eV^{-1} for **I1** to 0.52 eV^{-1} for **I7**. Therefore, phenoxazine and julolidine derivatives are electronically electronically softer and more polarizable compared with the phenyl, thiophene, benzothiophene, and fluorene derivatives. The chemical potential values became less negative from −4.42 eV for **I3** to −3.88 eV for **I7**. The more negative μ value of **I3** suggests a relatively greater tendency to accept electron density, which agrees with its high EA and stabilized LUMO energy. Conversely, the less negative chemical potential of **I7** reflects its strong electron-donating character and reduced electron-accepting tendency.

The electrophilicity index, ω, showed the highest value for **I3** at 8.84 eV, followed by **I2** and **I6**, with values of 8.52 and 8.49 eV, respectively. The high electrophilicity of **I3** indicates a relatively strong electrophilic character while maintaining a stable frontier orbital arrangement. This further supports the conclusion that **I3** provides the most balanced electronic profile among the investigated molecules. In contrast, **I7** showed the lowest electrophilicity index of 7.81 eV, consistent with its relatively destabilized frontier-orbital levels and lower voltage-related photovoltaic descriptors.

Overall, the global reactivity descriptor analysis confirms the donor-dependent modulation of the electronic structure. Weak and moderate donors such as phenyl, thiophene, benzothiophene, and fluorene preserve higher IP values and moderate hardness, whereas stronger donors such as phenoxazine and julolidine reduce IP and hardness while increasing softness. Although this enhanced softness may contribute to stronger electronic polarization and red-shifted absorption, it is also associated with HOMO destabilization and reduced V_{oc}. Among the investigated systems, **I3** bearing benzothiophene exhibits the most favorable combination of high Koopmans-based EA, high electrophilicity, low Eb, and suitable OPV-related descriptors, supporting its identification as the most promising molecular-level screening candidate in the present series.

Table 6: Global reactivity descriptors of molecules **I1**–**I7** estimated from frontier molecular orbital energies using Koopmans' approximation*

	IP	EA	η	μ	S	ω
I1	5.53	3.21	1.16	-4.37	0.43	8.23
I2	5.46	3.24	1.11	-4.35	0.45	8.52
I3	5.52	3.31	1.10	-4.42	0.45	8.84
I4	5.43	3.18	1.12	-4.30	0.44	8.22
I5	5.32	3.12	1.10	-4.22	0.45	8.08
I6	5.06	3.10	0.98	-4.08	0.51	8.49
I7	4.84	2.92	0.96	-3.88	0.52	7.81

*IP: ionization potential; EA: electron affinity; η: chemical hardness; μ: chemical potential; S: chemical softness; ω: electrophilicity index. IP, EA, η, μ, and ω are given in eV, whereas S is given in eV^{-1}.

4. CONCLUSION

In this study, donor-dependent structure–property relationships were systematically investigated for a series of isoindigo-based D–A–D small molecules using DFT and TD-DFT calculations. By varying the terminal donor units from weak aromatic donors to strongly electron-donating groups, we evaluated how donor strength and π-conjugation affect frontier orbital alignment, optical absorption, exciton binding, LUMO offset, and estimated voltage-related OPV descriptors.

The results reveal a clear design principle: the strongest electron donor does not necessarily yield the best overall OPV-related descriptor balance. Strong donor units such as phenoxazine and julolidine effectively narrow the HOMO–LUMO gap and shift the absorption toward longer wavelengths, reaching λmax values of 803 and 838 nm, respectively. However, these bathochromic shifts are accompanied by substantial HOMO destabilization, lower estimated V_oc values, and higher Eb values. Thus, excessive electron donation creates a trade-off between red-shifted absorption and voltage retention.

Among the investigated derivatives, the benzothiophene-substituted molecule I3 provided the most favorable balance of calculated descriptors. It combined strong absorption at 672.55 nm, the highest oscillator strength of the series, high LHE, the lowest Eb, a suitable LUMO offset, and a high estimated Voc. Thiophene-containing I2 and fluorene-containing I4 also showed balanced descriptor profiles, indicating that moderate donor strength and effective donor–bridge conjugation are more advantageous than excessive HOMO elevation. These findings suggest that benzothiophene and thiophene are particularly promising terminal donor units for future isoindigo-based small-molecule OPV design.

The present results should be interpreted as molecular-level screening guidelines rather than direct device-performance predictions. Intermolecular packing, π–π stacking, side-chain engineering, dielectric screening, blend morphology, charge mobility, and donor–acceptor interfacial effects were not explicitly included in the current isolated-molecule model. Future work should therefore combine the donor-selection strategy identified here with solvent and solid-state calculations, aggregate or dimer models, side-chain optimization, and experimental validation through UV–vis spectroscopy, electrochemical measurements, and device-oriented studies. Overall, the study highlights the importance of balancing absorption red-shift, exciton dissociation, and voltage preservation in the rational design of isoindigo-based organic photovoltaic candidates.

5. CONFLICT OF INTEREST

The authors declare no conflict of interest.

6. ACKNOWLEDGMENTS

The authors gratefully acknowledge the computational resources provided by TÜBİTAK ULAKBİM High Performance and Grid Computing Center (TRUBA).

7. REFERENCES

1. Rand BP, Genoe J, Heremans P, Poortmans J. Solar cells utilizing small molecular weight organic semiconductors. Prog Photovoltaics Res Appl. 2007 Dec 24;15(8):659–76. Available from: <URL>.

2. Bai H, Wang Y, Cheng P, Wang J, Wu Y, Hou J, et al. An electron acceptor based on indacenodithiophene and 1,1-dicyanomethylene-3-indanone for fullerene-free organic solar cells. J Mater Chem A. 2015;3(5):1910–4. Available from: <URL>.

3. Ostroverkhova O. Organic optoelectronic materials: Mechanisms and applications. Chem Rev. 2016 Nov 23;116(22):13279–412. Available from: <URL>.

4. Mishra A, Bäuerle P. Small molecule organic semiconductors on the move: Promises for future solar energy technology. Angew Chemie Int Ed. 2012 Feb 27;51(9):2020–67. Available from: <URL>.

5. Lin Y, Li Y, Zhan X. Small molecule semiconductors for high-efficiency organic photovoltaics. Chem Soc Rev. 2012 May 15;41(11):4245–72. Available from: <URL>.

6. Brédas JL, Norton JE, Cornil J, Coropceanu V. Molecular understanding of organic solar cells: The challenges. Acc Chem Res. 2009 Nov 17;42(11):1691–9. Available from: <URL>.

7. Bureš F. Fundamental aspects of property tuning in push–pull molecules. RSC Adv. 2014 Oct 22;4(102):58826–51. Available from: <URL>.

8. Roncali J. Molecular engineering of the band gap of π-conjugated systems: Facing technological applications. Macromol Rapid Commun. 2007 Sep 3;28(17):1761–75. Available from: <URL>.

9. Randell NM, Kelly TL. Recent advances in isoindigo-inspired organic semiconductors. Chem Rec. 2019 Jun 30;19(6):973–88. Available from: <URL>.

10. Stalder R, Mei J, Graham KR, Estrada LA, Reynolds JR. Isoindigo, a versatile electron-deficient unit for high-performance organic electronics. Chem Mater. 2014 Jan 14;26(1):664–78. Available from: <URL>.

11. Li J, Cao J, Duan L, Zhang H. Evolution of isoindigo-based electron-deficient units for organic electronics: From natural dyes to organic semiconductors. Asian J Org Chem. 2018 Nov 27;7(11):2147–60. Available from: <URL>.

12. Deng P, Zhang Q. Recent developments on isoindigo-based conjugated polymers. Polym Chem.

2014 Apr 15;5(10):3298–305. Available from: <URL>.

13. Zhang G, Fu Y, Xie Z, Zhang Q. Synthesis and photovoltaic properties of new low bandgap isoindigo-based conjugated polymers. Macromolecules. 2011 Mar 22;44(6):1414–20. Available from: <URL>.

14. Jung EH, Ahn H, Jo WH, Jo JW, Jung JW. Isoindigo-based conjugated polymer for high-performance organic solar cell with a high VOC of 1.06 V as processed from non-halogenated solvent. Dye Pigment. 2019 Feb 1;161:113–8. Available from: <URL>.

15. Mahmood K, Liu ZP, Li C, Lu Z, Fang T, Liu X, et al. Novel isoindigo-based conjugated polymers for solar cells and field effect transistors. Polym Chem. 2013 May 21;4(12):3563–74. Available from: <URL>.

16. Zhang H, Li Y, Zhang X, Zhang Y, Zhou H. Role of interface properties in organic solar cells: from substrate engineering to bulk-heterojunction interfacial morphology. Mater Chem Front. 2020 Oct 1;4(10):2863–80. Available from: <URL>.

17. Jiang BH, Wang YP, Liao CY, Chang YM, Su YW, Jeng RJ, et al. Improved blend film morphology and free carrier generation provide a high-performance ternary polymer solar cell. ACS Appl Mater Interfaces. 2021 Jan 13;13(1):1076–85. Available from: <URL>.

18. Shaheen A, Anwar N, Chen F, Chan Y, Xie H, Lee S. Materials interface engineering: Impact of interfacial molecular orientation on organic electronic devices. Adv Funct Mater. 2025 Nov 29;35(47):2505173. Available from: <URL>.

19. Yang Y, Liu Z, Zhang G, Zhang X, Zhang D. The effects of side chains on the charge mobilities and functionalities of semiconducting conjugated polymers beyond solubilities. Adv Mater. 2019 Nov 4;31(46):1903104. Available from: <URL>.

20. Wang E, Mammo W, Andersson MR. 25th anniversary article: Isoindigo-based polymers and small molecules for bulk heterojunction solar cells and field effect transistors. Adv Mater. 2014 Mar 12;26(12):1801–26. Available from: <URL>.

21. Venkateswararao A, Wong KT. Small molecules for vacuum-processed organic photovoltaics: Past, current status, and prospect. Bull Chem Soc Jpn. 2021 Mar 15;94(3):812–38. Available from: <URL>.

22. Chung HY, Oh J, Park JH, Cho I, Yoon WS, Kwon JE, et al. Spectroscopic studies on intramolecular charge-transfer characteristics in small-molecule organic solar cell donors: A case study on ADA and DAD triad donors. J Phys Chem C. 2020 Aug 27;124(34):18502–12. Available from: <URL>.

23. Karuppusamy M, Panneer SVK, Varathan E, Ravva MK, Easwaramoorthi S, Subramanian V. Design of isoindigo-based small-molecule donors for bulk heterojunction organic solar cell applications in combination with nonfullerene acceptors. J Phys Chem A. 2024 May 30;128(21):4206–24. Available from: <URL>.

24. Frisch MJ, Trucks GW, Schlegel HB, Scuseria GE, Robb MA, Cheeseman JR. Gaussian 16, Revision B.01. Wallingford CT: Gaussian, Inc.; 2019. Available from: <URL>.

25. Dennington R, Keith TA, Millam JM. GaussView 6.0. 16. Semichem Inc., shawnee mission. - References - Scientific research publishing. Semichem Inc., Shawnee Mission; 2016. Available from: <URL>.

26. Perdew JP, Wang Y. Accurate and simple analytic representation of the electron-gas correlation energy. Phys Rev B. 1992 Jun 15;45(23):13244–9. Available from: <URL>.

27. Ditchfield R, Hehre WJ, Pople JA. Self-consistent molecular-orbital methods. IX. An extended gaussian-type basis for molecular-orbital studies of organic molecules. J Chem Phys. 1971 Jan 15;54(2):724–8. Available from: <URL>.

28. Hariharan PC, Pople JA. The influence of polarization functions on molecular orbital hydrogenation energies. Theor Chim Acta. 1973 Sep;28(3):213–22. Available from: <URL>.

29. Clark T, Chandrasekhar J, Spitznagel GW, Schleyer PVR. Efficient diffuse function-augmented basis sets for anion calculations. III. The 3-21+G basis set for first-row elements, Li–F. J Comput Chem. 1983 Sep 7;4(3):294–301. Available from: <URL>.

30. Haridas R, Velore J, Pradhan SC, Vindhyasarumi A, Yoosaf K, Soman S, et al. Indoor light-harvesting dye-sensitized solar cells surpassing 30% efficiency without co-sensitizers. Mater Adv. 2021 Nov 29;2(23):7773–87. Available from: <URL>.

31. Scharber MC, Mühlbacher D, Koppe M, Denk P, Waldauf C, Heeger AJ, et al. Design rules for donors in bulk-heterojunction solar cells—Towards 10 % energy-conversion efficiency. Adv Mater. 2006 Mar 17;18(6):789–94. Available from: <URL>.

32. Park S, Jeong J, Hyun G, Kim M, Lee H, Yi Y. The origin of high PCE in PTB7 based photovoltaics: Proper charge neutrality level and free energy of charge separation at PTB7/PC71BM interface. Sci Rep. 2016 Oct 13;6(1):35262. Available from: <URL>.

33. Green MA. Solar cell fill factors: General graph and empirical expressions. Solid State Electron. 1981;24(8):788–9. Available from: <URL>.

34. Jindal V, Aldahdooh MKR, Gomez ED, Janik MJ, Milner ST. Tight-binding model predicts exciton energetics and structure for photovoltaic molecules. Phys Chem Chem Phys. 2024 May 29;26(21):15472–83. Available from: <URL>.

35. Lu T. A comprehensive electron wavefunction analysis toolbox for chemists, Multiwfn. J Chem Phys.

2024 Aug 28;161(8):082503. Available from: <URL>.

36. Koopmans T. Über die zuordnung von wellenfunktionen und eigenwerten zu den einzelnen elektronen eines atoms. Physica. 1934 Jan 1;1(1–6):104–13. Available from: <URL>.

37. Parr RG, Pearson RG. Absolute hardness: Companion parameter to absolute electronegativity. J Am Chem Soc. 1983 Dec 1;105(26):7512–6. Available from: <URL>.

38. Parr RG, Szentpály L v., Liu S. Electrophilicity Index. J Am Chem Soc. 1999 Mar 1;121(9):1922–4. Available from: <URL>.

39. Parr RG, Donnelly RA, Levy M, Palke WE. Electronegativity: The density functional viewpoint. J Chem Phys. 1978 Apr 15;68(8):3801–7. Available from: <URL>.

40. Becke AD. Density-functional exchange-energy approximation with correct asymptotic behavior. Phys Rev A. 1988 Sep 1;38(6):3098–100. Available from: <URL>.

41. Lee C, Yang W, Parr RG. Development of the Colle-Salvetti correlation-energy formula into a functional of the electron density. Phys Rev B. 1988 Jan 15;37(2):785–9. Available from: <URL>.

42. Becke AD. Density-functional thermochemistry. III. The role of exact exchange. J Chem Phys. 1993 Apr 1;98(7):5648–52. Available from: <URL>.

43. Yanai T, Tew DP, Handy NC. A new hybrid exchange–correlation functional using the Coulomb-attenuating method (CAM-B3LYP). Chem Phys Lett. 2004 Jul 21;393(1–3):51–7. Available from: <URL>.

44. Heyd J, Scuseria GE, Ernzerhof M. Hybrid functionals based on a screened Coulomb potential. J Chem Phys. 2003 May 8;118(18):8207–15. Available from: <URL>.

45. Chai JD, Head-Gordon M. Long-range corrected hybrid density functionals with damped atom–atom dispersion corrections. Phys Chem Chem Phys. 2008 Nov 28;10(44):6615–20. Available from: <URL>.

46. Hehre WJ, Ditchfield R, Pople JA. Self—consistent molecular orbital methods. XII. Further extensions of Gaussian—Type basis sets for use in molecular orbital studies of organic molecules. J Chem Phys. 1972 Mar 1;56(5):2257–61. Available from: <URL>.

47. Mei J, Graham KR, Stalder R, Reynolds JR. Synthesis of isoindigo-based oligothiophenes for molecular bulk heterojunction solar cells. Org Lett. 2010 Feb 19;12(4):660–3. Available from: <URL>.